INSTITUTE OF PHYSICS PUBLISHING JOURNAL OF PHYSICS: CONDENSED MATTER

J. Phys.: Condens. Matter **16** (2004) 5339–5348 PII: S0953-8984(04)75232-7

Crystal and magnetic structure of the $Ca_3Mn_2O_7$ Ruddlesden–Popper phase: neutron and synchrotron x-ray diffraction study

Maxim V Lobanov[1], Martha Greenblatt[1,8], El'ad N Caspi[2,3], James D Jorgensen[2], Denis V Sheptyakov[4], Brian H Toby[5], Cristian E Botez[6,7] and Peter W Stephens[6,7]

[1] Department of Chemistry and Chemical Biology, Rutgers University, Piscataway, NJ 08854, USA
[2] Materials Science Division, Argonne National Laboratory, Argonne, IL 60439, USA
[3] Physics Department, Nuclear Research Centre—Negev, PO Box 9001, 84190 Beer-Sheva, Israel
[4] Laboratory for Neutron Scattering, ETH Zürich and Paul Scherrer Institut, CH-5232 Villigen PSI, Switzerland
[5] NIST Center for Neutron Research, National Institute of Standards and Technology, Gaithersburg, MD 20899, USA
[6] Department of Physics and Astronomy, State University of New York, Stony Brook, NY 11794, USA
[7] National Synchrotron Light Source, Brookhaven National Laboratory, Upton, NY 11973, USA

Received 21 January 2004
Published 9 July 2004
Online at stacks.iop.org/JPhysCM/16/5339
doi:10.1088/0953-8984/16/29/023

Abstract

The crystallographic and magnetic structures of $Ca_3Mn_2O_7$ Ruddlesden–Popper phase have been determined by a combination of neutron and synchrotron x-ray diffraction. Two-phase behaviour observed at room temperature is attributed to an incomplete structural phase transition. The magnetic structure was solved in the $Cm'c2'_1$ Shubnikov group with dominant G-type antiferromagnetic order in the perovskite bilayers. The temperature evolution of the structural and magnetic parameters is presented.

1. Introduction

Recently, there has been a great deal of interest in complex manganese compounds exhibiting the colossal magnetoresistance (CMR) effect. Special attention has been paid to the layered Ruddlesden–Popper (RP) compounds, which have been shown to exhibit low-field CMR due to interplane tunnelling [1]. The $Ca_{3-x}La_xMn_2O_7$ system exhibits a rich magnetic phase diagram, where magnetic and transport properties are coupled to subtle crystallographic distortions through symmetry restrictions on the weak ferromagnetic (WFM) ordering. A crossover from

[8] Author to whom any correspondence should be addressed.

weak ferromagnetism to a magnetic state without a ferromagnetic component was observed for $x \approx 0.35$ by dc magnetization [2].

The parent compound itself, $Ca_3Mn_2O_7$, exhibits WFM, and the orthorhombic distortion that is responsible for this effect has been demonstrated in a recent single-crystal x-ray diffraction study [3]. The space group proposed was $Cmc2_1$; the symmetry lowering was attributed to an octahedral tilting distortion. The tilting pattern corresponds to the $(\Phi\Phi\Psi_z)/(\Phi\Phi\Psi_z)$ tilt system in the notation of Aleksandrov and Bartholome [4], or $a^-a^-c^+/a^-a^-c^+$ in the more conventional Glazer notation [5]. A recent investigation of $Ca_{3-x}La_xMn_2O_7$ ($x = 0$–0.4) by electron diffraction [6] indicated that the crystal structure at room temperature is orthorhombic with either $Cmc2_1$ or $Cmcm$ space group symmetry over the entire composition range studied, where the $Cmcm$ model corresponds to a more symmetric $(\Phi\Phi 0)/(\Phi\Phi 0)$ tilt system without a z-component. The $Cmcm$ structural model has also been used to fit neutron diffraction data for $Ca_2LaMn_2O_7$ [7].

Recently, a model for the evolution of the magnetic structure as a function of dopant concentration (x) was proposed for the related compounds, $Ca_{1-x}Th_xMn_2O_7$, based on symmetry considerations and variations of structural parameters [8]. The model predicts a magnetic structure transformation from G-type (in Wollan–Koehler, WC [9] notation) where all nearest-neighbour couplings are antiferromagnetic (AF), to C-type, where the perpendicular-to-plane coupling is ferromagnetic (FM). This kind of transformation has been directly observed for the $Sr_{3-x}La_xMn_2O_7$ by neutron diffraction [10].

In the present work, we report the crystallographic structure of $Ca_3Mn_2O_7$ at room temperature, studied by complementary time-of-flight (TOF) neutron powder diffraction and synchrotron x-ray powder diffraction (SXD) measurements. We also report the nuclear and magnetic structure of $Ca_3Mn_2O_7$ as a function of temperature, investigated by means of constant wavelength (CW) neutron powder diffraction and SXD.

2. Experimental details

A powder $Ca_3Mn_2O_7$ sample was prepared by the citrate sol–gel technique with annealing in oxygen flow, as described in [2]. The oxygen content was determined by inverse redox titration with Mohr salt and $KMnO_4$ [11].

CW neutron diffraction (ND) experiments were performed with the BT-1 diffractometer at NIST with a neutron wavelength of 1.5398(1) Å, produced by a Cu(311) monochromator. TOF neutron diffraction experiments were performed with the special environment powder diffractometer (SEPD) [12] at the intense pulsed neutron source (IPNS) at Argonne.

Room temperature SXD data were collected with the powder diffractometer located at the Materials Sciences Beamline X04SA of the Swiss Light Source (SLS) at the Paul Scherrer Institut. The sample was placed in a 0.5 mm glass capillary, which was continuously rotated perpendicular to the scattering plane. X-rays of 0.953 73 Å wavelength were selected by a double-crystal Si(111) monochromator and calibrated with a $Na_2Al_2Ca_3F_{14}$ standard. After being diffracted from the powder sample, the beam was analysed with a five-channel, Si(111) multi-crystal analyser detector. Variable temperature SXD data were collected on the SUNY X3B1 beamline, at the National Synchrotron Light Source (NSLS), Brookhaven National Laboratory. The sample was mounted on a closed-cycle He cryostat on a flat plate, in θ–2θ reflection geometry. X-rays of wavelength 1.1497 Å were selected by a double-crystal Si(111) monochromator and calibrated using a NIST1976a corundum standard. After being diffracted from the powder sample, the beam was analysed with a Ge(111) crystal. X-ray scattering intensities were collected at room temperature, as well as at 160, 115, 80, 40, 25 and 20 K, in steps of 0.005°, by counting for 2 s at every 2θ, for selected angular ranges. In both

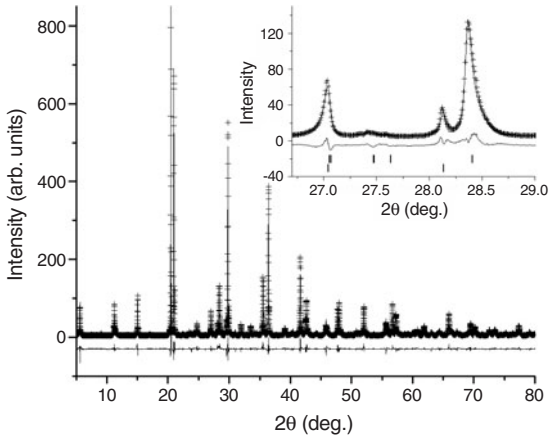

Figure 1. Experimental, calculated and difference patterns for the Rietveld refinement of room temperature synchrotron x-ray diffraction data using a two-phase refinement model ($Cmc2_1$ + $I4/mmm$) with the peak shift and asymmetry correction described in the text. Inset: selected region of the spectrum, showing pronounced peak asymmetry (tails). The two sets of tick marks correspond to the $Cmc2_1$ (top) and $I4/mmm$ (bottom) phases.

synchrotron experiments, the intensity of the incoming beam was monitored by an ion chamber and normalized for the decay of the primary beam.

The GSAS [13] program with the EXPGUI interface [14] was used for the refinements of crystallographic and magnetic structures from the ND data. For the modelling of *hkl*-dependent effects seen in the high-resolution SXD data, the Topas [15] program was utilized. A cylindrical absorption correction as defined in [16] was employed for the SXD data.

3. Results and discussion

3.1. Crystallographic structure at room temperature

The neutron diffraction patterns could be indexed based on a C-centred orthorhombic unit cell, as reported previously [3]. However, the high resolution SXD showed that, at room temperature, the sample actually consists of a mixture of two phases, with closely related lattice parameters and about 10% abundance of the minor phase. The difference between the two phases is beyond the resolution of both laboratory x-ray and neutron diffraction. A Le Bail profile fit [17] with a single-phase $Cmc2_1$ model yielded a reasonable fit to the TOF data (SEPD, high resolution backscattering bank): $\chi^2 = 3.7$, $R_{wp} = 8.37\%$, where the imperfections in the model could largely be attributed to the stacking faults, as discussed further below. However, with the exceptional resolution of the X04SA instrument, the peaks from each phase are clearly resolved and were indexed as tetragonal $I4/mmm$ (minority) and orthorhombic $Cmcm$ or $Cmc2_1$ (majority) (figure 1).

Attempts to fit the SXD data with a higher $Cmcm$ symmetry model for the majority phase yielded anomalously high atomic displacement parameters (ADPs) for the oxygen atoms, providing evidence for the presence of an additional tilting component. The choice of the lower symmetry $Cmc2_1$ model is also supported by the refinement of the TOF neutron diffraction data. The $Cmcm$ model yielded $\chi^2 = 12.5$, $R_{wp} = 15.36\%$ and anomalously large ADPs for oxygen atoms, in particular $B_{iso}(O2) = 5.8$ Å^2. The $Cmc2_1$ model provides a significantly better refinement, $\chi^2 = 8.1$, $R_{wp} = 12.36\%$, as well as reasonable values for the ADPs. The higher than expected values of the reliability factors originate from stacking fault effects that

Table 1. Positional and thermal parameters of atoms and Mn–O interatomic distances (Å) from the Rietveld refinement of room temperature diffraction data. Upper table: majority phase ($Cmc2_1$; neutron diffraction—SEPD). Lower table: minority phase ($I4/mmm$, synchrotron x-ray diffraction).

Atom	Site	x	y	z	B_{iso}
$Cmc2_1$ (no. 36): $a = 19.4462(6)$, $b = 5.2453(2)$, $c = 5.2399(2)$					
Ca1	4a	1/2	0.752(2)	0.744(2)	0.9(1)
Ca2	8b	0.3135(2)	0.753(1)	0.775(1)	1.34(8)
Mn1	8b	0.0974(2)	0.753(2)	3/4	0.66(6)
O1	4a	0	0.700(1)	0.756(2)	0.91(9)
O2	8b	0.0882(2)	0.0391(9)	−0.039(1)	1.75(8)
O3	8b	0.1044(2)	0.5338(9)	0.027(1)	1.89(8)
O4	8b	0.1952(2)	0.7807(7)	0.747(1)	0.87(6)
Mn–O1: 1.914(5); Mn–O2: 1.871(9), 1.876(8); Mn–O3: 1.910(9), 1.857(8); Mn–O4: 1.907(6)					
$I4/mmm$ (no. 139): $a = 3.69185(5)$, $c = 19.6254(5)$					
Ca1	2b	0	0	1/2	0.7(2)
Ca2	4e	0	0	0.3145(3)	0.5(2)
Mn	4e	0	0	0.0978(3)	0.5(1)
O1	2a	0	0	0	2.2(2)
O2	4e	0	0	0.194(1)	=B(O1)
O3	8g	0	1/2	0.1019(9)	=B(O1)
Mn–O1: 1.919(6); Mn–O2: 1.889(6); Mn–O3: 4 × 1.848(1)					

cannot be modelled using GSAS. Attempts to introduce a second $I4/mmm$ minority phase into the refinement, as was done in the SXD fit, required a large number of constraints and neither improved agreement factors, nor produced significant ($>2\sigma$) changes in the structural parameters of the majority orthorhombic phase. This is not unexpected, since the diffraction features between the two phases are completely unresolved with the ND data (see below). The atomic coordinates for the majority $Cmc2_1$ phase obtained from a single-phase ND and two-phase SXD fits are identical within errors; accordingly, we present in table 1 the ND results for the majority $Cmc2_1$ phase and SXD results for the minority $I4/mmm$ one. Finally, a trace ($\sim$0.7%) amount of an impurity phase (identified as $n = 1$ RP, $Ca_2MnO_{4-\delta}$) was detected and introduced into the final refinements. The refined fraction of $I4/mmm$ phase is 9.5(1)%.

Two additional diffraction features are seen clearly with the exceptional resolution of the present SXD data. The first effect is a small but systematic shift of reflections with large h ('long axis') indices from their theoretical positions, and the second is a strongly asymmetric peak shape for certain reflections, with relatively broad tails on either side. Both features are commonly observed in systems with stacking faults [18], which are typically present in various RP compounds because of their layered structures [19]. However, at present, there is (to our knowledge) no Rietveld program that allows introduction of corresponding corrections in relation to microstructural properties. Using the Topas code, we therefore applied refineable individual peak shifts to selected peaks with high h values as well as 'circle convolution' ($1 - \sqrt{|\varepsilon_m/\varepsilon|}$, $0 \leqslant \varepsilon \leqslant \varepsilon_m$) asymmetries for the peaks with pronounced tails. Only peaks in the majority (orthorhombic) phase were corrected. This yielded a significant improvement of the SXD fit: with this correction the Rietveld refinement yielded reliability factors of $\chi^2 = 16.3$ and $R_{wp} = 11.66\%$, compared to $\chi^2 = 31.4$ and $R_{wp} = 16.30\%$ without these corrections. The experimental, calculated and difference patterns are shown in figure 1. No significant anisotropic peak broadening (that could result from the smaller size of domains along the stacking a-direction) was detected.

The R-factor values are still high, mainly because of remaining imperfections in the description of shift and asymmetry effects. Refinements of occupancy factors and/or anisotropic ADPs did not yield any significant improvement of the fit. The thermal evolution of ADPs showed evidence for static disorder (see below), plausibly associated with two possible senses of the Ψ_z octahedral tilt component. Evidence for disorder effects has been found in a recent transmission electron microscopy (TEM) study [20]. We attempted to model the disorder by a split-site model using the CW 115 K neutron data set to avoid the bias induced by the unresolved $I4/mmm$ minority phase present at the RT on the magnitudes of 'observed' structure factors. Low angle reflections, which might have non-negligible magnetic contribution, were excluded from the data. Similar models were used previously to refine the structure of $Sr_3Ru_2O_7$ with a $Bbcb$ ($00\Phi_z/00\Phi_z$) symmetry [21], and to model the tetrahedral chain disorder (also realized as two possible senses of rotation) in the Ca_2MnGaO_5 brownmillerite [22]. Following [6], octahedral tilt modifies the O2 and O3 atomic coordinates as

$$\begin{aligned} &\text{O2(8b)} : x_0 + \Delta_x, \qquad 0 + \delta_y, \qquad 0 - \delta_z \\ &\text{O3(8b)} : x_0 - \Delta_x, \qquad 1/2 + \delta_y, \qquad 0 + \delta_z, \end{aligned}$$

where x_0 is the z-coordinate in the parent $I4/mmm$ structure, Δ_x originates from the majority (Φ) tilt, $\delta_y = \frac{1}{4}(\cos\Psi_z - 1)$ and $\delta_z = \frac{1}{4}\sin\Psi_z$, while other atomic positions are not explicitly affected by Ψ_z. Note that the sign for the y-coordinate displacement of the O3 atom is changed compared to [6], where a possible misprint is present. Accordingly, O2 and O3 oxygen positions were split, and constraints were imposed on the oxygen positions, to maintain equal magnitudes of $\pm\Psi_z$ tilts. This model led to no improvement in the R-factor values, and the refined fraction of minority 'enantiomer' is 4.8(6)%, close to that (4.1%) found in the $Sr_3Ru_2O_7$ structure [21]. However, it yielded slightly more realistic values of ADPs for the O2 and O3 atoms (0.72 and 0.60 Å^2, respectively, as compared to 0.83 and 0.75 Å^2 for a 'not split' model). A model of 'local $Cmcm$ symmetry', i.e. a similar split-site model with a refineable fraction of '$Cmcm$-type' atoms (i.e. with $y, z = 0$, corresponding to $\Psi_z = 0$), was also attempted, and also failed to produce a superior fit.

It is likely that the actual structure involves some complicated ordering of 'enantiomeric configurations', similar to what was identified in the Sr_2MnGaO_5 brownmillerite by TEM [23] and modelled in a $Ima2(00\gamma)s00$ superspace symmetry and modulation vector $q = 1/2c^*$, while earlier high resolution neutron diffraction studies claimed either $Ima2$ or $Imma$ symmetry, providing a simplified (averaged) description of the structure. Alternatively, the discrepancy can be attributed to the presence of stacking faults, which is established from the observed hkl-dependent shifts and asymmetries of the reflections.

4. Magnetic structure determination

Magnetic reflections appear in the neutron diffraction patterns below $T_N \approx 115$ K. They can be indexed on the basis of the orthorhombic ($Cmc2_1$) crystallographic cell, and two possible indexations are possible: the former assumes propagation vector $k = 0$, and accordingly the magnetic reflections are indexed as ($l01$) for l even and ($l10$) for l odd. The latter adopts $k = (100)$ (Y point of the Brillouin zone), and the corresponding indexation is ($l10$) for l even and ($l01$) for l odd. The pseudotetragonal lattice prevents an unambiguous distinction between those possibilities (e.g., by means of Le Bail fits); however, the observation of weak ferromagnetism (established by magnetic susceptibility measurements) allowed us to conclude that the former indexing scheme is correct (zero propagation vector is a prerequisite for the WFM [24]). Moreover, the experimentally observed intensity of the 'forerunner' (100)

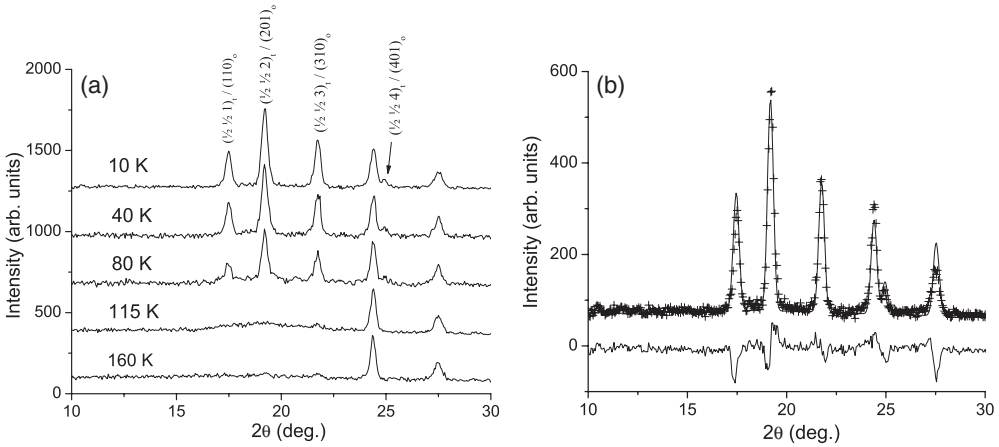

Figure 2. (a) Low angle part of the CW neutron diffraction data (BT-1) as a function of temperature. Miller indices of the main magnetic reflections are shown in both parent tetragonal (subscript 't') and orthorhombic ('o', assuming propagation vector $k = 0$) settings. (b) Rietveld refinement of the 10 K data in the $Cm'c2'_1$ model; only the same low angle part with significant magnetic contribution is shown.

reflection is zero, although it is not a sufficient proof by itself (the intensity could vanish due to a geometrical factor).

It is instructive to index the magnetic reflections on the basis of the parent tetragonal ($I4/mmm$) cell, which is related to the orthorhombic cell by the relations $a_o \sim c_t$; $b_o \sim c_o \sim a_t\sqrt{2}$, where the subscripts 'o' and 't' indicate orthorhombic and tetragonal, respectively, and they can be accordingly reindexed as $(1/2\ 1/2\ l)_t$. The appearance of $(1/2\ 1/2\ l)_t$ reflections shows that the dominant magnetic contribution is either G type or C type, i.e., with an AF arrangement of the moments within the bilayer plane (the tetragonal ab-plane perpendicular to the stacking axis). However, this single observation does not allow us to determine a unique magnetic structure from the eight possible (for the $Cmc2_1$ crystallographic symmetry) magnetic groups, because each of them corresponds to a superposition of three different orderings (for three spin components), and it turns out that every magnetic group contains at least one component which transforms as either C or G type.

Therefore, symmetry conditions for weak ferromagnetism (WF) were employed in the search for the possible magnetic structures. It turns out that only three of the eight possible magnetic groups allow WFM, namely $Cm'c2'_1$, $Cmc'2'_1$ and $Cm'c'2_1$ [25]. They correspond to the ($G_xF_yC_z$), ($F_xG_yA_z$) and ($A_xC_yF_z$) spin configurations in WC notation. The WC symbol in the case of the RP phases is not unique, because only spin arrangements within individual bilayers are accounted for. Hence, for each WC spin configuration, there are two magnetic groups, which differ by the relative orientations of the moments in sequential bilayers. There are in total six magnetic groups derived from the $Cmc2_1$ crystallographic group that allow some F component for the individual bilayers. However, for three of these, the moments of the sequential bilayers cancel each other, and there is no macroscopic ferromagnetism.

Rietveld refinements performed for the other three models with the lowest temperature (10 K) dataset showed that the $Cm'c2'_1$ model ($G_xF_yC_z$) provided the best fit to the experimental data, and, consequently, it was used for the analysis of the temperature dependence of magnetic parameters. The refinement is not sensitive to the 'minority' magnetic components (F_y and C_z). Identical values of reliability factors are obtained for the refinements with only the x-component

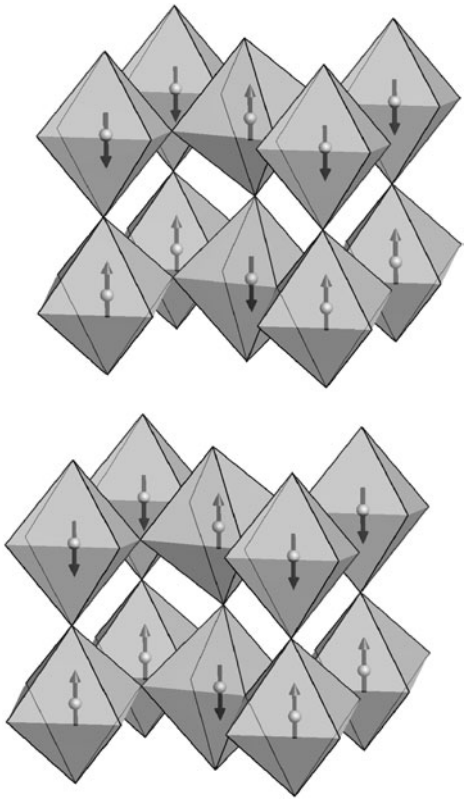

Figure 3. Schematic representation of the crystallographic and magnetic structure of $Ca_3Mn_2O_7$. Ca atoms are not shown for clarity. Only the majority (G_x) component of the magnetic moment is shown.

(G_x) or with all three components allowed, and the refined magnitudes of the yz-components are small and refined with a large error: $\mu_y = 0.4(2)\ \mu_B$, $\mu_z = 0.3(3)\ \mu_B$. Therefore, only the x-component was refined in the analysis of the variable temperature datasets. Clearly, the existence of a WF component in the magnetization requires a nonzero y (FM) component of the ordered moment. However, it is small and cannot be reliably refined from powder data. The refined crystallographic and magnetic structure of $Ca_3Mn_2O_7$ is shown in figure 3.

The orientation of the magnetic moment along the stacking axis ($a_o = c_t$) is consistent with the trend observed for the $Sr_{3-x}La_xMn_2O_7$ [10], where the azimuthal angle θ of spin canting from the c_t direction in the similar predominantly G-type structure was shown to increase monotonically with increasing x and is equal to 8° for the $Sr_3Mn_2O_7$ composition. Moreover, upon the isoelectronic substitution of Pr^{3+} for La^{3+} in the $(La_{1-z}Pr_z)_{1.2}Sr_{1.8}Mn_2O_7$ series, the rotation of the easy magnetization axis from the ab-plane to the c-axis was observed; i.e., the decrease of the A-cation size favours the c_t moment orientation [26]. Interestingly, orientation of the moment along the y-direction (in the orthorhombic $Pbca$ structure; c is the stacking axis) was reported for the $Ca_4Mn_3O_{10}$ [27].

5. Temperature evolution of structural and magnetic parameters

In both SXD experiments, low angle peaks had a full width at half maximum (FWHM) of ∼0.07°, which is significantly larger than the instrument resolution of the diffractometers. The peak broadening in the room temperature SXD data was found to be dominated by size (Scherrer) contributions (L_x component of the TCH pseudo-Voigt function) for both phases, and

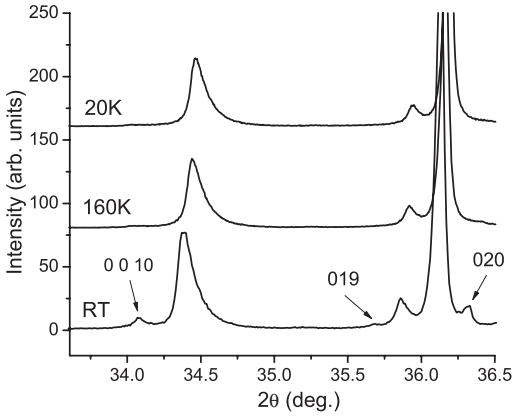

Figure 4. Selected regions of synchrotron diffraction patterns (NSLS) at room temperature (RT), 160 and 20 K, evidencing two-phase behaviour at RT and single-phase behaviour at low temperature. Miller indices for $I4/mmm$ phase reflections are shown.

corresponding 'Lorentzian sizes' estimated with the Scherrer equation are 310 and 260 Å for the orthorhombic and tetragonal phases, respectively. This broadening prevents the detection of the two phases by means of neutron diffraction. A likely origin of such behaviour is that the sample consists of small domains of orthorhombic and tetragonal phases, as a result of an incomplete structural phase transition. Indeed, the low temperature SXD data show a single $Cmc2_1$ phase (figure 4). The tetragonal-to-orthorhombic transition occurring in the 200–300 °C range was indeed observed in the study of $Ca_{3-x}La_xMn_2O_7$ by electron microscopy [6]. However, it was not possible to distinguish whether it occurred as a single transition or as a sequence of group-maximal subgroup transformations according to the symmetry tree $I4/mmm \rightarrow Fmmm \rightarrow Cmcm \rightarrow Cmc2_1$. In our experiments, we found coexisting $I4/mmm$ and $Cmc2_1$ phases at room temperature, while we did not find any evidence for the presence of 'intermediate' $Fmmm$ or $Cmcm$ phases either at room temperature or in low T data. Therefore, our data appear to be in favour of a single-transition hypothesis.

The $Cm'c2'_1$ model found from the analysis of the 10 K data was used to fit the magnetic structure, with only the main (G_x) component of the magnetic moment being refined. The thermal evolution of the lattice parameters and the ordered magnetic moment is presented in figures 5(a) and (b). The lattice parameters decrease monotonically with decreasing temperature, and no pronounced anomaly (e.g., change of slope) is detected at T_N. The magnitude of the orthorhombic distortion $\eta = \frac{b_o - c_o}{b_o + c_o}$ is nearly constant over the entire temperature range. The refined Mn–O–Mn bond angles are also essentially constant at low ($T \leqslant 160$ K) temperature, and do not show significant anomalies at T_N. Thus, the magnitude of the octahedral tilt does not change significantly with temperature. The average Mn–O–Mn bond angle is 162.3° at room temperature and lies within the 160.6°–160.9° range at low T.

According to dc magnetic susceptibility data, the compound undergoes a transition into an AFM state at $T_N \approx 110$ K. The neutron diffraction pattern collected at $T = 115$ K shows magnetic diffuse scattering which manifests itself as a broad maxima centred at the positions where sharp magnetic peaks develop at lower temperature, thus implying short-range ordered magnetic correlations already at this temperature (figure 2(a)). The presence of reflections with nonzero l index indicates that the short-range order is not essentially 2D. However, it is not meaningful to make quantitative estimates of the ordered moments because of the small peak intensities and large widths. The temperature dependence of ADPs yielded larger than

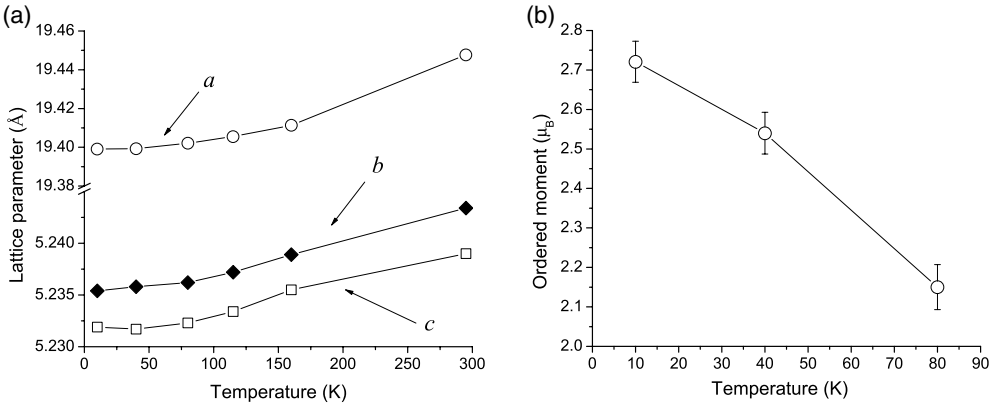

Figure 5. Temperature evolution of the lattice parameters (a) and ordered magnetic moment (b), as refined from neutron diffraction data. Only the majority (G_x) component of the magnetic moment was refined. Curves are guides to the eye.

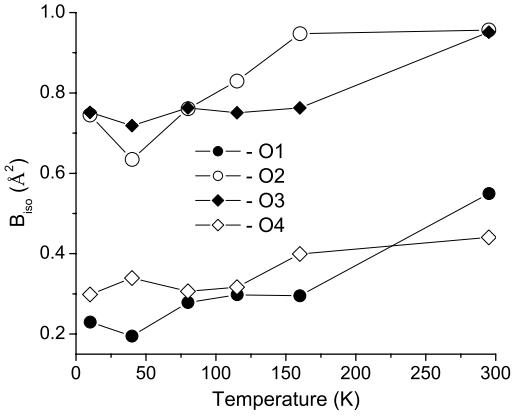

Figure 6. Temperature evolution of the isotropic displacement parameters for oxygen atoms ($Cmc2_1$ model) indicating the presence of significant static disorder. Curves are guides to the eye.

expected values at $T = 10$ K, especially for the oxygen atoms: $B_{\rm iso}(\mathrm{O2}) \approx B_{\rm iso}(\mathrm{O3}) \approx 0.8$ Å^2 (figure 6). This provides evidence for the presence of static disorder (described above), which in turn can result in a reduced magnitude of the ordered magnetic moment, the observed value for which, 2.67(5) $\mu_{\rm B}$ at 10 K, is well below the theoretical value of 3 $\mu_{\rm B}$.

6. Conclusions

Detailed neutron and synchrotron diffraction study of $Ca_3Mn_2O_7$ has shown that at room temperature the compound is a two-phase mixture of majority orthorhombic (space group $Cmc2_1$) and minority tetragonal ($I4/mmm$) phases, with the latter having a weight fraction of ∼9.5%. This behaviour apparently originates from an incomplete structural transition occurring upon the decrease of temperature. This conclusion is supported by synchrotron diffraction experiments at low temperature which show a single $Cmc2_1$ phase. The orthorhombic distortion is produced by tilts of MnO_6 octahedra, and the refined Mn–O–Mn bond angles show significant deviations from the ideal 180° values. The presence of static disorder was revealed from the thermal evolution of atomic displacement parameters. hkl-dependent peak asymmetry and shifts, attributed to stacking faults, were observed in the high resolution synchrotron x-ray diffraction data, and incorporated into the Rietveld refinements.

The compound undergoes a transition into an AFM state at $T_N \approx 110$–115 K. The low T magnetic structure was solved from neutron diffraction data utilizing symmetry conditions for weak ferromagnetism, and was refined in the $Cm'c2'_1$ Shubnikov group, corresponding to the $G_xF_yC_z$ spin configuration with a dominant G-type antiferromagnetic order in the perovskite bilayers.

Acknowledgments

The authors are grateful to A Kern, A Leineweber, G Popov and T Emge for helpful discussions. The work at Rutgers was supported by the National Science Foundation grant DMR-0233697. The work at Argonne was supported by the US Department of Energy, Office of Science, Division of Materials Sciences, under contract No W-31-109-ENG-38. This work was partly performed at the Swiss Light Source, Paul Scherrer Institute, Villigen, Switzerland. The research carried out at the NSLS at Brookhaven was supported by the US Department of Energy, Division of Materials Sciences and Division of Chemical Sciences. The SUNY X3 beamline at NSLS was supported by the Division of Basic Energy Sciences of the US Department of Energy under grant No DE-FG02-86ER45231.

Certain trade names and company products are identified in order to specify experimental procedures adequately. In no case does such identification imply recommendation or endorsement by the National Institute of Standards and Technology, nor does it imply that the products are necessarily the best available for the purpose.

References

[1] Kimura T, Tomioka Y, Kuwahara H, Asamitsu A, Tamura M and Tokura Y 1996 *Science* **274** 1698
[2] Fawcett I D, Kim E, Greenblatt M, Croft M and Bendersky L A 2000 *Phys. Rev.* B **62** 6485
[3] Guiblin N, Grebille D, Leligny H and Martin C 2002 *Acta Crystallogr.* C **58** i3
[4] Aleksandrov K S and Bartholome J 1994 *J. Phys.: Condens. Matter* **6** 8219
[5] Glazer A M 1972 *Acta Crystallogr.* B **28** 3384
[6] Bendersky L A, Chen R, Fawcett I D and Greenblatt M 2001 *J. Solid State Chem.* **157** 309
[7] Green M A and Neumann D A 2000 *Chem. Mater.* **12** 90
[8] Lobanov M V, Li S and Greenblatt M 2003 *Chem. Mater.* **15** 1302
[9] Wollan E O and Koehler W C 1955 *Phys. Rev.* **100** 545
[10] Ling C D, Millburn J E, Mitchell J F, Argyriou D N, Linton J and Bordallo H N 2000 *Phys. Rev.* B **62** 15096
[11] Vogel A I 1996 *Qualitative Inorganic Analysis* (London: Longman)
[12] Jorgensen J D, Faber J, Carpenter J M, Crawford R K, Haumann J R, Hittermann R L, Kleb R, Ostrowski G E, Rotella F J and Worlton T G 1989 *J. Appl. Crystallogr.* **22** 321
[13] Larson A C and Von Dreele R B 1994 *Los Alamos National Laboratory Report* LAUR 86-748
[14] Toby B H 2001 *J. Appl. Crystallogr.* **34** 210
[15] Cheary R W and Coelho A A 1992 *J. Appl. Crystallogr.* **25** 109
[16] Sabine T M, Hunter B A, Sabine W R and Ball C J 1998 *J. Appl. Crystallogr.* **31** 47
[17] Le Bail A, Duroy H and Fourquet J L 1988 *Mater. Res. Bull.* **23** 447
[18] See, for example, Scardi P, Leoni M and Dong Y H 2000 *Eur. Phys. J.* B **18** 23
[19] Sloan J, Battle P D, Green M A, Rosseinsky M J and Vente J F 1998 *J. Solid State Chem.* **138** 135
[20] Bendersky L A, Greenblatt M and Chen R 2003 *J. Solid State Chem.* **174** 418
[21] Shaked H, Jorgensen J D, Chmaissem O, Ikeda S and Maeno Y 2000 *J. Solid State Chem.* **154** 361
[22] Abakumov A M, Rozova M G, Pavlyuk B Ph, Lobanov M V, Antipov E V, Lebedev O I, Van Tendeloo G, Sheptyakov D V, Balagurov A M and Bourée F 2001 *J. Solid State Chem.* **158** 100
[23] Abakumov A M, Alekseeva A M, Rozova M G, Antipov E V, Lebedev O I and Van Tendeloo G 2003 *J. Solid State Chem.* **174** 319
[24] Turov E A 1965 *Physical Properties of Magnetically Ordered Crystals* (New York: Academic) chapter 5
[25] Opechowski W and Guccione R 1965 *Magnetism* vol IIA, ed G T Rado and H Suhl (New York: Academic) p 105
[26] Vasil'ev A, Voloshok T, Apostu M, Suryanarayanan R and Revcolevschi A 2001 *JETP Lett.* **73** 630
[27] Battle P D, Green M A, Lago J, Millburn J E, Rosseinsky M J and Vente J F 1998 *Chem. Mater.* **10** 658